The influence of rotor geometry on power transfer between rotors in gerotor-type screw compressors

Matthew G. Read
Email: m.read@city.ac.uk

Nikola Stosic
Email: n.stosic@city.ac.uk

Ian K. Smith
Email: i.k.smith@city.ac.uk

Department of Mechanical Engineering and Aeronautics
City, University of London
Northampton Square, London, UK

ABSTRACT

A configuration of twin-screw positive displacement machine is proposed, consisting of an internally-geared outer rotor meshing with an externally-geared inner rotor. Helical rotors with constant profile and pitch are used with parallel rotor axes and stationary end plates incorporating inlet and discharge ports to achieve internal compression or expansion. The focus of this paper is to understand the effect of rotor geometry on two key performance indicators; the swept volume of the machine, and the proportion of input power transferred between the inner and outer rotors. This requires a detailed analysis of the limitations on rotor profile generation, the formation of working chambers, and the forces exerted on the rotors. The choice of rotor for power transfer to or from the machine is shown to be an important consideration, and helical rotors are found to enable lower power transfer between rotors during operation when compared to straight-cut rotors, but with reduced swept volume for the same machine size. For particular applications, this compromise is characterised through multi-objective optimisation of the rotor profile and wrap angle in order to identify appropriate configurations for the proposed machine.

1 Introduction

An externally-geared inner rotor can mesh with an internally-geared outer rotor such that points of continuous contact are achieved during rotation, creating variable-volume working chambers. These internal-mesh rotors can be used in various configurations of pump. Gerotor pumps use straight-cut co-rotating rotors with fixed and parallel axes. Progressing cavity pumps use helical profiles with the outer 'rotor' held stationary, requiring the inner rotor to rotate about its own axis while orbiting around the fixed axis of the outer stator. The application of gerotor type profiles as compressors with either straight or helical rotors has not previously been rigorously investigated. The potential of these machines is currently unknown as a large number of geometrical and operational parameters will influence performance, making optimisation a significant challenge. Existing rotor profiling methods can be applied in combination with a thermodynamic model of the compression process to characterise these machines. The aim of this paper is to understand the effect of rotor geometry on the working chamber volume and rotor torques, and investigate the compromise between maximising flow rate and minimising power transfer between rotors through multi-objective optimisation of the rotor profiles and wrap angles.

Conventional internal-mesh machines such as gerotor pumps are widely used in automotive and aerospace fuel and oil pumping applications [1], while progressing cavity pumps are often used in industrial application involving high viscosity or multiphase fluids [2]. Moineau [3] was among the first to describe methods of defining rotor geometries suitable for the progressing cavity pump, while also proposing the use of rotors based on epi & hypocycloids with variable pitch or variable profile in order to achieve internal compression of the working chamber between inlet and discharge of the machine. Adams & Beard [4] considered basic geometrical features of helical rotors formed from epi & hypotrochoids. More recent developments have looked at implementing the concept of conical internally-geared rotors for compressor applications [5].

There are considerable challenges in manufacturing rotors of this type with the requisite high accuracy using efficient and economical methods, and a simpler configuration using constant pitch and profile rotors with stationary porting has been proposed by the authors [6]. In this configuration, both rotors are allowed to rotate about fixed and parallel axes. With open ends, this configuration can only function as a pump. However, the use of fixed end plates with porting allows control over the periods during which fluid can enter and leave the working chamber, as illustrated in Fig. 1. The design of this port geometry is dependent on the rotor shape and the required compression ratio, and is discussed in previous work by the authors which has characterised the port flow areas and their influence on pressure losses during filling and discharge of the working chamber [7, 8]. As with conventional gerotor pumps and screw compressors, the gap between end plates and rotor faces will be small in a practical machine in order to limit leakage flows. By closing the working chamber from both ends of the machine for a controlled period during which the volume is varying, the machine can operate as either a compressor or expander. This gerotor-type screw configuration has a number of potential advantages over conventional twin-screw machines, including reduced leakage areas, co-directional thermal expansion, stiffer rotors, and reduced sliding velocity in clearance gaps. A common feature of progressing cavity pumps and the proposed internally-geared screw compressor

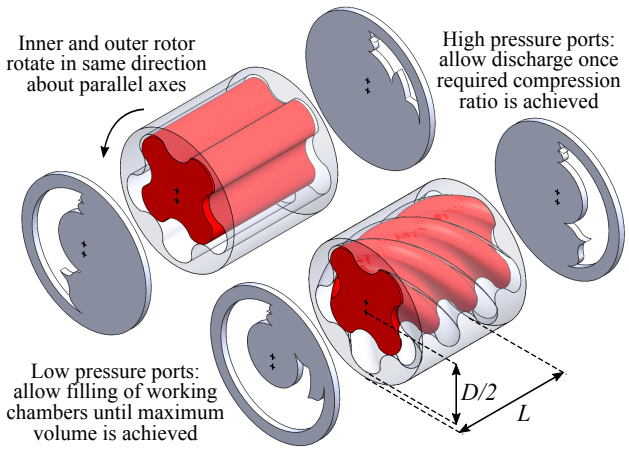

Fig. 1: Exploded diagram illustrating co-rotating internally-geared compressors with either straight or helical rotors, and with inlet and discharge porting on fixed end plates. Rotor length, L, maximum profile diameter, D, and compression volume ratio are the same in both cases.

is the requirement for the minimum cross-sectional area of the working chamber to be zero, as any non-zero value will create a direct leakage path connecting nominally separate chambers. Fully conjugate inner and outer rotor profiles are therefore required. This is not necessarily the case for gerotor pumps with straight rotors, which can function well with a non-conjugate fillet profile, resulting in a non-zero clearance volume. However, an important feature of the rotor profiles for all these machines is the requirement for continuous contact between rotors, which allows the formation of enclosed working chambers whose volume varies with the angular position of the rotors.

There is a wealth of literature on the generation and optimisation of rotor profiles for gerotor pump applications. Colborne [9] was among the first to study gerotor gear profiles and defined performance parameters based on geometry. Beard [10, 11] compared epi & hypotrochoidal profiles for pumping applications, while Shung and Pennock [12] refined the analytical approach used to define rotor profiles, and more recently Tong et al. [13, 14] have described a general method for investigating rotors with non-circular internal pitch. Investigation of the effect of rotor profiles on pump performance have been presented by Hsieh [15–17] for various types of cycloid and trochoid, Bonandrini et al. [18] for epi & hypotrochoid profiles, and Mimmi [19] for profiles generated from a range of fundamental curves. More recently, methods have been described for defining profiles consisting of multiple curve sections [20], and using a generating ellipse with variable coefficient [21], while asymmetric gerotor profiles are described by Jacazio & De Martin [22], with discussion of their possible benefits for pumping applicatons. For all rotor generation methods, undercutting must be avoided to ensure practical profiles with continuous contact between rotors. Conditions leading to singularities in the inner gear profile of a cycloidal gerotor were identified by Litvin and Feng [23] through application of gearing theory; this approach was developed by Vecchiato et al. [24], while Mimmi & Pennacchi [25] have considered undercutting conditions from a geometrical perspective. There is, perhaps surprisingly, very limited literature discussing the use of gerotor type machines in compression or expansion applications. Beard et al. [10] state that the gerotor profiles discussed are suitable for pumps and compressors but focus on general geometrical features, while Mathias et al. [26] describe experimental measurements of a gerotor expander using R123 working fluid where performance was found to be comparable with a scroll type machine. While there are many

studies investigating the thermodynamic performance of gerotor pumps (a comprehensive review is provided by Rundo [1], and design tools are described by Gamez-Montero et al. [27,28]), no literature could be found regarding the thermodynamic analysis of gerotor machines with internal compression or expansion.

Wear is an important consideration for gerotor pumps due to the potentially high contact forces between the rotors. Clearance between rotors is an important factor [29, 30], and the influence of rotor profile on wear has been investigated [22,31], while possible profile modifications to limit wear have also been described [32] and variable clearance distributions have been proposed to reduce pressure and stress fluctuations [33]. The aim of the current study is to investigate whether the proposed helical internally-geared compressor can be designed in order to limit the rotor-to-rotor contact forces that cause wear to occur by minimising the power transfer between rotors. While much of the literature focussed on gerotor pump applications has investigated profiles with non-zero clearance volumes [1, 22, 31, 32], the approach for generating fully-conjugate cycloidal profiles described by Vecchiato [24] is applied in the current study. An interesting point to note is that while Beard et al. [4, 10, 11] and Bonandrini et al. [18] consider similar fully-conjugate profiles, a minimum working chamber volume is defined along with a compression ratio. It will be shown in this paper that these profiles do in fact have a minimum working chamber cross-sectional area, and hence volume, of zero, and are therefore suitable for the proposed helical compressor application. The method of profile generation is summarised in the following section, and key features and limitations of these profiles are discussed.

2 Description of circular pin-generated rotor profiles

Internal pin-generated gearing can be used to generate meshing rotor profiles. Continuous contact points are achieved when the inner gear contains one less or one more lobe than the outer gear. It is possible to generate two types of cycloidal gearing in this way:

(i) An extended epicycloid profile is generated on the gear with the smaller centrode when the profile of the gear with larger centrode is partially defined by a circular pin,
(ii) An extended hypocycloid profile is generated on the gear with the larger centrode when the profile of the gear with smaller centrode is partially defined by a circular pin.

The geometry and position of the pins on a rotor consisting on N_1 lobes can be defined in the coordinate system S_1 as shown in Fig. 2. By rotating this profile in the coordinate system of a second rotor, S_2, with a parallel but non-coincident axis and $N_2 = N_1 \pm 1$ lobes, the profile of this second rotor, ψ_2, can be found by application of the equation of meshing as described in detail by Vecchiato [24], whose nomenclature is followed here. The geometry used to generate the rotor profiles is illustrated in Fig. 2 for the case when $N_1 > N_2$. This result also allows ψ_{1p}, the section of rotor profile ψ_1 defined by the circular arc of the pin (i.e. when $\theta_{min} \leq \theta \leq \theta_{max}$) to be defined. Rotation of ψ_2 in coordinate system S_1 then generates the conjugate profile (or fillet), ψ_{1q}, that connects the sections of circular profile in order create a complete rotor profile, ψ_1, that achieves multiple points of continuous contact with ψ_2. Alternatively, a non-conjugate fillet section can be defined for ψ_{1q}; any arbitrary profile can be defined as long as it does not infringe on the conjugate profile, which would result in interference between the rotors. While this may simplify manufacturing of the rotors, it results in a non-zero minimum area for the working chambers formed. The choice of fillet profile is an important consideration for machines with either straight or helical rotors, and is discussed further in Section 2.1. When considering the generation of rotor profiles, an important parameter is the gearing ratio, $m_{21} = \omega_2/\omega_1 = N_1/N_2$. Extended epicycloid and hypocycloid profiles can both be generated using this method when $m_{21} > 1$ (as shown in Fig. 2) or $m_{21} < 1$ respectively. The extended epicycloidal gearing profile with $m_{21} > 1$ and contact on the inner flank of the pin has previously been identified as appropriate for gerotor pumps [10, 24], and is considered here for compressor applications using both straight and helical rotors. Examples of possible profiles are shown in Fig. 3; these profiles are defined by the lobe number N_1, the non-dimensional geometric parameters $\lambda = a/r_1$ and $\sigma = \rho/r_1$, and the axis spacing distance $E = r_1/N_1$. There are some limitations on the values of these parameters which are discussed in more detail in Sections 2.3 and 2.4. The maximum diameter of the outer rotor profile, D, can be determined by considering that, in all cases, the maximum diameter of the inner rotor occurs when $\phi_1 = \pi$ and $\theta = 0$; once the inner rotor has turned a further half revolution, the tips of the inner and outer rotors must be coincident for a conjugate fillet profile, leading to the definitions in Eqn. 1. In Fig. 3 the value of E has been adjusted in order to achieve the same maximum outer profile diameter for all cases.

$$\frac{E}{D} = \frac{1}{2N_1(\lambda - \sigma + 2/N_1)}, \quad \frac{a}{D} = \lambda N_1 \left(\frac{E}{D}\right), \quad \frac{\rho}{D} = \sigma N_1 \left(\frac{E}{D}\right) \tag{1}$$

2.1 Influence of outer rotor fillet profile

For compressors with straight rotors, minimum volume should correspond with the point when the high pressure port closes and discharge ceases. A non-zero minimum volume is allowable, but the opening of the low pressure port should be

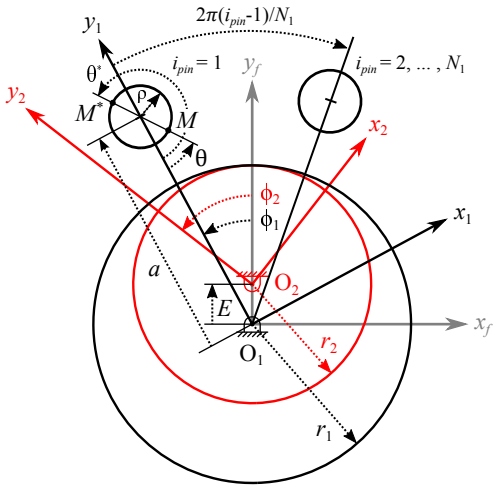

Fig. 2: Overcentrode extended epicycloid profile generation (i.e. $m_{21} > 1$ and the pin profile forms part of ψ_1) showing geometry and position of circular pins in coordinate system S_1 and possible contact points on inner (M) and outer (M^*) pin flanks

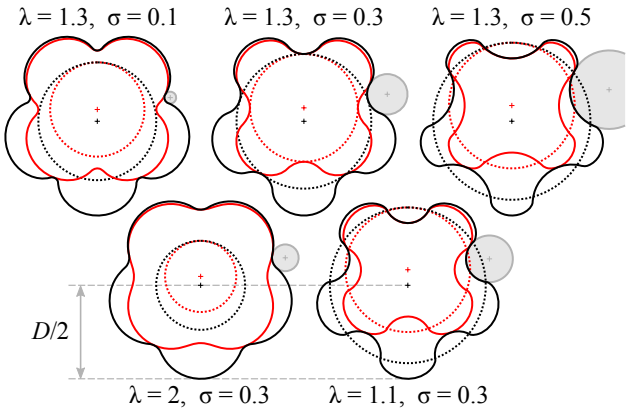

Fig. 3: Examples of pin-generated rotor profiles (solid lines) and centrodes (dashed lines) with $N_1 = 5$ and specified values of λ and σ. All profiles are shown with the same value of D, and the generating pin is shown in grey

delayed until the high pressure fluid remaining in the working chamber has been expanded to the suction pressure in order to recover some of the compression work.

For compressors with helical rotors, however, a non-zero minimum area creates a direct path for fluid to flow from the high to low pressure ends of the machine via working chambers either side of the throat formed at the axial location of the minimum area (see Fig. 4). In order to effectively seal the working chambers from each other, the minimum working chamber area should therefore be zero, which is only possible using fully conjugate profiles. The clearance volume is therefore also zero for this configuration. In order to compare the characteristics of positive displacement machines with straight and helical rotors, the profiles discussed in this paper all use conjugate fillet profiles. A rigorous investigation of the behaviour of the rotor-to-rotor contact points and the resulting formation of working chambers has been performed. This is particularly important as it clarifies that the working chamber area starts from, and returns to, zero, as required for screw type machines.

2.2 Rotor contact points and working chamber formation

Using the coordinates defined in Fig. 2, for rotor position ϕ_1 there exists one contact point between ψ_{1p} and ψ_2. The rotation of the pin in coordinate system S_2 and application of the equation of meshing is sufficient to completely define ψ_2 [24]. For a general point, P_2 on ψ_2 it is again possible to solve the equation of meshing to identify the angular position of the rotors, ϕ'_1, at which P_2 is a contact point on:

(i) ψ_{1p} (the pin section of ψ_1), occurring when $\phi'_1 = \phi'_{1p}$. Note that this is the trivial solution where: $\phi'_{1p} = \phi_1$ for $i_{pin} = 1$ and $\phi'_{1p} = \phi_1 + 2\pi(1 - 1/N_1)$ for $i_{pin} = 2$.

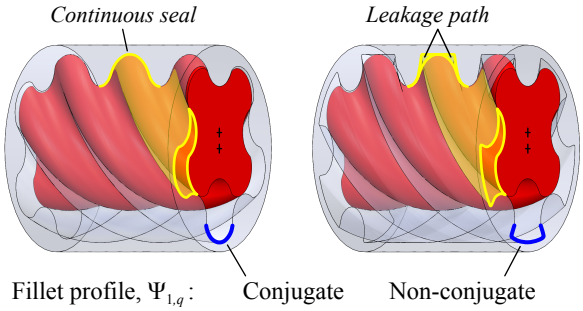

Fig. 4: Illustration of working chamber formation (highlighted in yellow) for helical rotors with and without conjugate outer rotor fillet profiles, and the leakage path created in the latter due to non-zero minimum cross-sectional area

(ii) ψ_{1q} (the fillet section of ψ_1), occurring when $\phi'_1 = \phi'_{1q}$. Note that the number of solutions depends on ϕ_1 and the pin geometry.

For any value of ϕ_1 it is therefore possible to find all values of ϕ'_1 and hence identify the position of all contact points on both the pin and fillet sections of ψ_1. The function $\phi'_{1q}(\phi_1)$ depends on the number and radial location of the pins as defined by the parameters N_1 and λ. Depending on the values of N_1 and λ there are a number of possible scenarios, with up to three fillet contact points occurring simultaneously, as illustrated in Fig. 5. The initial angle at which the working chamber forms, $\phi_{1,i}$, is found as the minimum value of ϕ_1 across the range of values of ϕ'_1. This is always less that π/N_1, and the working chamber here is a single contact point with zero area. As ϕ_1 increases, the two (or more) simultaneous contact points on the pin and/or fillet sections of ψ_1 define the sections of each rotor profile that form the bounds of the working chambers, and the area can then be calculated as a function of rotor position. Due to the symmetry of the rotor lobe profiles, the way in which

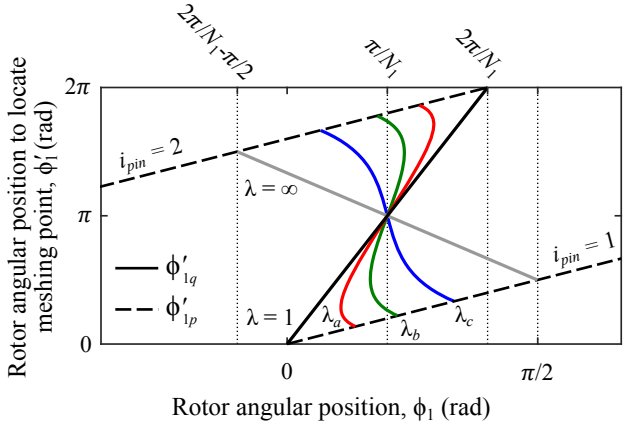

Fig. 5: General description of fillet contact points as a function of rotor lobe number, N_1, and normalised radial pin position, λ (results shown for case when $N_1 = 5$, $\lambda_a = 1.1$, $\lambda_b = 1.3$, $\lambda_c = 2$)

the working chamber area reduces to zero at the end of the cycle is identical to this pattern of working chamber formation, but mirrored around the rotor position $\phi_1 = \pi(1 + 1/N_1)$ (where the working chamber reaches its maximum area), resulting in a final position for the working chamber, $\phi_{1,f}$, as defined in Eqn. 2. An example of the working chamber area for the rotor profile in Fig. 3 with $\lambda = 1.3$ and $\sigma = 0.5$ is shown in Fig. 6. The normalised working chamber area, $\bar{A}_{wc}$, is defined by dividing the working chamber area by the area of a circle enclosing the outer rotor profile, as shown in Eqn. 3.

$$\phi_{1,f} = 2\pi(1 + 1/N_1) - \phi_{1,i} \tag{2}$$

$$\bar{A}_{wc} = 4A_{wc}/(\pi D^2) \tag{3}$$

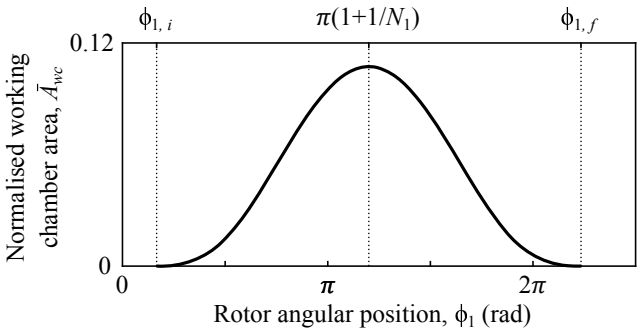

Fig. 6: Normalised working chamber area, $\bar{A}_{wc}$, as function of rotor position for $N_1 = 5$, $\lambda = 1.3$ and $\sigma = 0.5$

2.3 Limiting values of pin geometry

It is interesting to note that the curves of ϕ_1' as a function of ϕ_1 illustrated in Fig. 5 are not functions of the normalised pin diameter, σ, but only depend on N_1 and λ. There are however limits on the range of values of σ that achieve the requirement of continuous contact between rotors. If the value of σ is too large then singularities can occur in the solution of the meshing equation, indicating that undercutting occurs during the generation of the profile ψ_2. This is described in detail for the case of overcentrode extended epicycloidal gearing by Vecchiato et al. [24], where the conditions that lead to singularities are defined by Eqn. 4.

Singularities occurs when: $\sigma - \zeta(\phi_1) \geq 0$ where

$$\zeta(\phi_1) = \frac{(1-m_{21})(1+\lambda^2-2\lambda\cos\phi_1)^{3/2}}{\lambda^2(1-m_{21})-m_{21}+\lambda(2m_{21}-1)\cos\phi_1} \quad (4)$$

It is therefore possible to define the range of values of σ that result in the generation of rotor profiles with no undercutting as $0 < \sigma < \sigma_{lim}$. When meshing occurs on the inner flank of the pin, $\sigma_{lim} = \min(\zeta)$ for range of ϕ_1 values where $\zeta > 0$. The value of σ_{lim} as a function of $(\lambda - 1)$ and N_1 can therefore be calculated, as shown in Fig. 7. In all cases, $\sigma_{lim} \to 0$ as

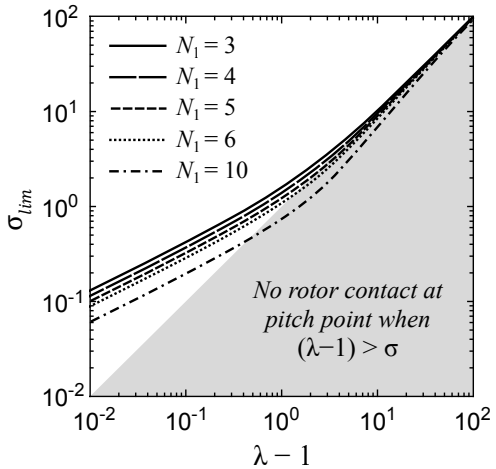

Fig. 7: Value of σ_{lim} as a function of $(\lambda - 1)$ and N_1 for extended epicycloid gearing with inner flank pin contact, showing the maximum possible pin diameter that avoids undercutting in profile ψ_2, and conditions resulting in no contact at pitch point

$\lambda \to 1$, meaning that a value of $a < r_1$ will always result in undercutting of the ψ_2 profile. The case when $\sigma = 0$ and $\lambda = 1$ corresponds to the special case of epicycloid profiles on both the inner and outer rotors. As the value of σ_{lim} varies with N_1 and λ, it is useful to define a normalised pin diameter ratio, $\bar{\sigma} = \sigma/\sigma_{lim}(N_1, \lambda)$, when comparing machine performance across a range of geometries. A value of $\bar{\sigma} = 1$ therefore corresponds to the maximum possible pin diameter for the chosen rotor geometry.

2.4 Pressure angle of pin generated cycloidal profiles

In conventional gearing for power transmission applications, the pressure angle, defined as the angle between the common tangent to the profiles and the line connecting the origins and the pitch point, indicates the load carrying capacity of the gears. The use of modified rotor profiles to limit contact to locations with low pressure angle have been investigated for gerotor pumps [29, 32]. The use of helical rotors, however, allows further restriction of the contact to the region of the pitch point. With reference to Fig. 2, rotor contact at the pitch point only occurs if $(a-\rho) \leq r_1 \equiv (\lambda-1) \leq \sigma$. The examples shown in Fig. 3 clearly illustrate this condition, which is important as pure rolling contact between the rotors only occurs at the pitch point, with some degree of sliding occurring at all other contact points. From Fig. 7 it can be seen that minimising the sliding between rotors further limits the range of σ values that can be chosen for a given value of λ.

When the above condition is met with helical rotors, a pitch length of less than half the rotor length ensures that at least two locations have contact at the pitch point for all rotor positions. As with conventional twin screw machines, a clearance distribution can be defined to ensure power transfer only occurs at these points [34]. The pressure angle, α_p, when the contact point coincides with the pitch point, can be expressed as shown in Eqn. 5.

$$\cos(\alpha_p + \pi/2) = \frac{1}{2\sigma}\left(1+\sigma^2-\lambda^2\right) \tag{5}$$

In twin screw machines it is useful to minimise the power transmission between rotors in order to minimise wear, which can adversely affect the clearance gaps, and hence the leakage and efficiency of the machine. The varying pressure within the working chambers of these machines means however, that it is not possible to completely eliminate power transmission between the rotors. Other factors such as the swept volume of the machine may also lead to compromises in the selection of rotor profiles, as discussed in the following section. If power transmission between the rotors is significant then timing gears may be necessary in order to eliminate rotor-to-rotor contact, although this adds to the complexity and cost of the machine. The ability of the rotors to transmit power with low pressure angle via rolling rather than sliding contact may therefore be an important consideration.

3 Compressor geometry with straight and helical rotors

Positive displacement machines can be formed using the rotor profiles described in Section 2. For helical rotors an additional geometric parameter is the wrap angle, Φ, defined as the angle through which the profile is rotated along the length of the rotor. The ratio of the inner and outer rotor wrap angles must match the gearing ratio such that $\Phi_2/\Phi_1 = m_{21}$. As with conventional screw compressors, the wrap angle of the rotors influences the swept volume and the forces exerted on the rotors [35, 36]. These are key factors in assessing the size, efficiency and reliability of the proposed internally-geared compressor, and are highly dependent on the rotor geometry. There is shown to be an inherent compromise between maximising flow rate and minimising power transfer between rotors. This relationship is characterised through multi-objective optimisation of the rotor profile and wrap angle, as discussed in the following sections.

As in gerotor pumps, pressure pulsations are considered to be an issue in compressors due to the resulting noise and vibrations. While increasing the number of lobes on the driven rotor will increase the frequency and potentially reduce the magnitude of pressure fluctuations, another important factor is the appropriate selection of volume ratio to avoid over or under compression. For conventional screw compressors, the specific power of the machine is usually the key design criteria, and driven rotors with 3, 4 and 5 lobes are used for both air and refrigeration applications [34]; a similar range of N_1 values has therefore been considered in the present study.

3.1 Working chamber volume

To assess the swept volume of the internally-geared machines it is necessary to understand how the volume of a single working chamber changes with rotor position, and how this contributes to the overall capacity of the machine. The calculation method for the working chamber volume depends on whether the rotors are straight or helical, as discussed below.

3.1.1 Volume with straight rotors

For internally-geared machines with straight rotors, the volume of a working chamber can easily be defined as the product of the working chamber cross-sectional area as a function of rotor position, $A_{wc}(\phi_1)$, and the rotor length, L. The swept volume, V_{sw}, is defined here as the volume created within the machine per revolution of the outer rotor, and is equal to the product of N_1 and maximum volume of a single working chamber. This can be presented as a normalised swept volume, $\bar{V}_{sw}$, defined as the swept volume divided by the total volume of the cylinder enclosing the outer rotor profile, as shown in Eqn. 6.

$$\bar{V}_{sw} = V_{sw}/V_{cyl} = \max(A_{wc}) \times 4N_1/(\pi D^2) \tag{6}$$

The contour map in Fig. 8 shows $\bar{V}_{sw}$ and α_p as functions of λ and $\bar{\sigma}$ for the case when $\Phi = 0$ and $N_1 = 5$. Note that the values of $\bar{V}_{sw}$ and α_p are always maximum when $\bar{\sigma} = 1$; this was found to be true for all values of N_1 considered in this paper. These results allow the actual swept volume to be calculated for a particular profile and specified values of L and D.

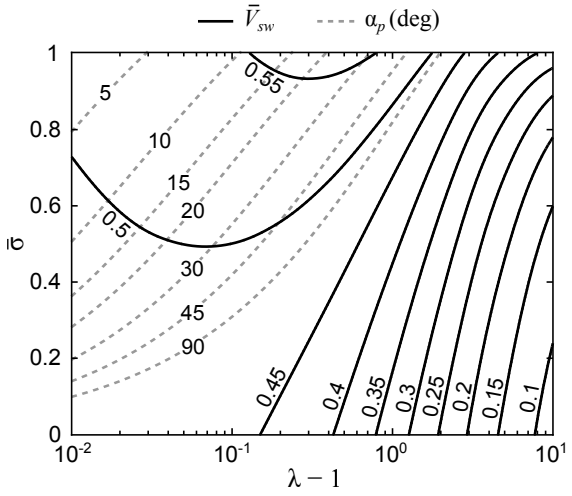

Fig. 8: Contour map showing normalised swept volume, $\bar{V}_{sw}$, and pitch point pressure angle, α_p, as a function of λ and $\bar{\sigma}$ for profiles with $N_1 = 5$ and $\Phi_1 = 0$ (i.e. straight rotors)

3.1.2 Volume with helical rotors

For the internally-geared configuration with helical rotors, the working chamber area must be integrated along the longitudinal length of the working chamber in order to find the volume for a given rotor position. This requires the wrap angle, Φ, of the helical rotors to be specified along with the rotor length, L. While helix angle can also be used to define rotor geometry, wrap angle has been used as the variable in this study as it will be shown that results for swept volume and rotor torque can be normalised by functions of rotor length and diameter, allowing non-dimensional results to be presented which are independent of the L/D ratio of the rotors. The sign convention adopted here locates the origin on the low pressure end face, with the longitudinal coordinate, z, increasing in the direction of the high pressure end of the rotors. The integral can be performed with respect to z, where the cross-sectional area of a particular working chamber can be defined at all points along the rotor length for a given rotor position. Alternatively, the integral can be performed with respect to the rotor angular position, ϕ_1, where the cross-sectional areas of the working chamber at the two end faces of the rotors (denoted $[A_{wc}]_{lp/hp}$) can be used to determine the volume for a general rotor position, $\phi_{1,g}$ (where $\phi_{1,i} < \phi_{1,g} \leq \phi_{1,f}$), as defined in Eqn. 7.

$$V_{wc}(\phi_{1,g}) = \int_0^L A_{wc}(\phi_1, z)dz = \frac{L}{\Phi_1}\int_{\phi_{1,i}}^{\phi_{1,g}} \left([A_{wc}]_{lp} - [A_{wc}]_{hp}\right)d\phi_1 \quad (7)$$

The integral of $[A_{wc}]_{lp}$ describes how the working chamber grows from zero volume, beginning at the low pressure end face of the compressor. With semi-infinite rotors, this working chamber would reach a maximum volume at the point where $[A_{wc}]_{lp}$ returns to zero; by subtracting the integral of the area at the high pressure end face, $[A_{wc}]_{hp}$, the volume of the working chamber that has passed beyond this plane is removed, resulting in the true, truncated working chamber volume. When $\Phi_1 < (\phi_{1,f} - \phi_{1,i})$ the working chamber volume reaches a maximum at the midpoint between the rotor positions at which $[A_{wc}]_{lp}$ and $[A_{wc}]_{hp}$ are maximum, corresponding to $\phi_1 = \pi(1 + 1/N_1) + \Phi_1/2$. Rather than calculate the working chamber volume for a specific rotor length, this volume can again be normalised by the volume of a cylinder enclosing the profile ψ_1 as discussed in Section 3.1.1.

When considering the helix wrap angle of the rotors, it can be seen that if the wrap angle of the outer rotor, $\Phi_1 \geq (\phi_{1,f} - \phi_{1,i})$, then a working chamber can be completely contained between the two rotors, and is never exposed to both rotor end faces simultaneously. This is a requirement for open-ended internal screw pumps and progressing cavity pumps to ensure that no direct path exists for liquid to flow from high to low pressure. In a compressor application this means that

the working chamber will never be exposed at the low pressure end face when the volume reaches maximum or during the ensuing compression, hence this face can be completely open to the low pressure supply.

If $\Phi_1 < (\phi_{1,f} - \phi_{1,i})$ then there will be some exposure of the working chamber to the low pressure end face at the point where the working chamber volume is maximum and compression begins. A shaped port is then required at the low pressure end to close off the working chamber from the supply at this point. An example of this can be seen in Fig. 1.

As the values of $\phi_{1,i}$ and $\phi_{1,f}$ depend on the rotor profiles, it is useful to define a normalised helical rotor wrap angle, $\bar{\Phi}_1$, as shown in Eqn. 8. A value of $\bar{\Phi}_1 = 1$ corresponds to the case when a complete working chamber can just be contained within the length of the rotors. This provides a rigorous basis for comparing geometrical characteristics of different configurations.

$$\bar{\Phi}_1 = \frac{\Phi_1}{\phi_{1,f} - \phi_{1,i}} = \frac{\Phi_1}{2\pi(1 + 1/N_1 - \phi_{1,i}/\pi)} \tag{8}$$

The material volume of the rotors themselves depends only on the profile and the rotor length. The instantaneous volume of fluid contained between the two rotors and the end face planes is therefore independent of wrap angle. Increasing the wrap angle does however result in a smaller maximum volume for a single working chamber and a smaller maximum value of $dV_{wc}/d\phi_1$. Therefore, less fluid is drawn into the working chambers with each revolution, and the swept volume is reduced. This is illustrated in Fig. 9a which shows $\bar{V}_{sw}$ as functions of $\bar{\Phi}_1$ and λ for profiles with $N_1 = 5$; in order to achieve the maximum swept volume possible, $\bar{\sigma} = 1$ has been used in all cases. The effect of the outer rotor lobe number, N_1, on the swept volume is illustrated in Fig. 9b. The results in Fig. 9 show that increasing the value of either $\bar{\Phi}_1$ or N_1 causes a reduction

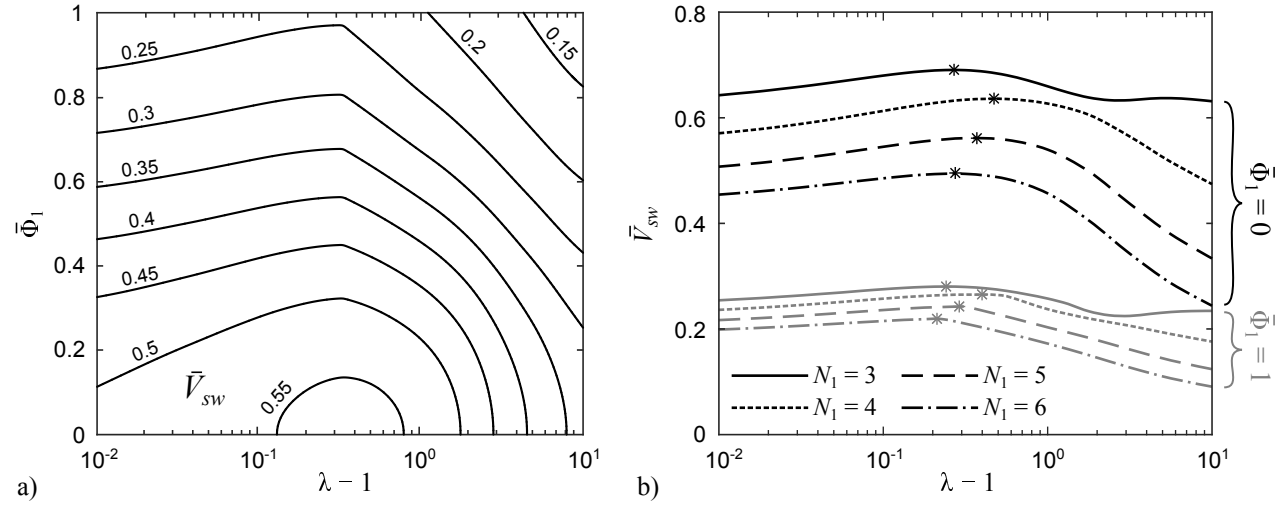

Fig. 9: a) $\bar{V}_{sw}$ as function of λ and $\bar{\Phi}_1$ for helical rotors with $N_1 = 5$ and $\bar{\sigma} = 1$ (note that $\bar{\Phi}_1 = 0$ corresponds to the straight rotor case shown in Fig. 8 when $\bar{\sigma} = 1$), and b) $\bar{V}_{sw}$ as function of λ for helical rotors with $N_1 = 3 \ldots 6$, $\bar{\sigma} = 1$ and $\bar{\Phi}_1 = 0$ and $\bar{\Phi}_1 = 1$, with maximum $\bar{V}_{sw}$ indicated by $*$ symbol

in the maximum achievable swept volume of an internally-geared machine of specified dimensions, and the maximum values of $\bar{V}_{sw}$ are seen to occur with values of $\bar{\sigma} = 1$ and λ in the range $1.2 - 1.5$. However, in order to decide on appropriate values for these parameters, the forces and torques acting on the rotors should also be considered.

4 Rotor forces and power transfer

The pressure inside the working chamber at a given rotor position will exert a resultant force on both rotors. The components of this force, $[F_x, F_y, F_z]$, can be found by considering the projected area of the working chamber on each rotor in the xy, xz and yz planes. It is also important to identify the centroids of these projected areas in order to resolve the torques and bearing reaction forces acting on the rotors. The terminology used to define the projected area and centroid coordinates is A_k and $[\bar{x}, \bar{y}, \bar{z}]_k$ respectively, where k is the projected plane (i.e. xy, xz or yz). From this definition it is apparent that $\bar{z}_{xy} = \bar{y}_{xz} = \bar{x}_{yz} = 0$.

The forces acting on the rotors are equal and opposite (Eqn. 9) but act about different axes of rotation; note that the axes of rotation are defined as z and z' for the outer and inner rotors respectively, where z' is parallel to z but passes through O_2. The torques acting on the rotors are therefore different as shown in Eqn. 10, and are a function of the rotor profiles and the

angular position of the rotors. The projected areas and centroids for machines with straight and helical rotors are discussed in the following sections.

$$\begin{bmatrix} F_{x,1} \\ F_{y,1} \end{bmatrix} = p_{wc} \begin{bmatrix} A_{yz} \\ -A_{xz} \end{bmatrix} = - \begin{bmatrix} F_{x,2} \\ F_{y,2} \end{bmatrix} \tag{9}$$

$$T_{z,1} = F_{y,1}\bar{x}_{xz} - F_{x,1}\bar{y}_{yz} \quad \text{and} \quad T_{z',2} = F_{y,2}\bar{x}_{xz} - F_{x,2}(\bar{y}_{yz} - E) \tag{10}$$

4.1 Straight rotors

For the case of a machine with straight rotors, the projected area for the force acting on the rotors due to pressure is the line joining the leading and trailing contact points of the working chamber, $[x,y]_\ell$ and $[x,y]_t$ respectively, multiplied by the rotor length, L. This leads to the definitions in Eqns. 11 and 12, and the force and torque exerted on each rotor can found by substitution in Eqns. 9 and 10.

$$A_{xz} = L(x_\ell - x_t) \quad \text{and} \quad A_{yz} = L(y_\ell - y_t) \tag{11}$$

$$\bar{x}_{xz} = \frac{1}{2}(x_\ell + x_t)\,, \quad \bar{y}_{yz} = \frac{1}{2}(y_\ell + y_t) \quad \text{and} \quad \bar{z}_{xz} = \bar{z}_{yz} = \frac{L}{2} \tag{12}$$

4.2 Helical rotors

As with the volume calculation described in Section 3.1.2, the integration required to find the projected areas and centroids for helical rotors can be performed in terms of the rotor angular position, ϕ_1, by considering the geometric conditions at the high and low pressures end faces. For a general rotor position, $\phi_{1,g}$, the projected area and associated centroid coordinates can be found as illustrated in Eqns. 13 to 15 for the xz plane.

$$A_{xz} = \frac{L}{\Phi_1} \int_{\phi_{1,i}}^{\phi_{1,g}} \left(\big[(x_\ell - x_t)\big]_{lp} - \big[(x_\ell - x_t)\big]_{hp} \right) d\phi_1 \tag{13}$$

$$\bar{x}_{xz} = \frac{L}{2A_{xz}\Phi_1} \int_{\phi_{1,i}}^{\phi_{1,g}} \left(\big[(x_\ell^2 - x_t^2)\big]_{lp} - \big[(x_\ell^2 - x_t^2)\big]_{hp} \right) d\phi_1 \tag{14}$$

$$\bar{z}_{xz} = \frac{L^2}{A_{xz}\Phi_1^2} \int_{\phi_{1,i}}^{\phi_{1,g}} \Big((\phi_{1,g} - \phi_1)\big[(x_\ell - x_t)\big]_{lp} - (\phi_{1,g} - \phi_1 + \Phi_1)\big[(x_\ell - x_t)\big]_{hp} \Big) d\phi_1 \tag{15}$$

These calculations can be repeated for the projection of the rotor contact lines in the yz plane in order to find the corresponding centroid coordinates and the rotor forces in the x direction. The components of force exerted on each rotor about their axis of rotation and the resulting rotor torques can then be found by again using Eqns. 9 and 10.

4.3 Working chamber pressure

The force and torque equations described in Sections 4.1 and 4.2 can be applied to the range of rotor geometries considered in Section 3.1 once the pressure of the working fluid as a function of rotor position is known. Detailed thermodynamics models developed for pump and screw compressor applications have demonstrated the importance of leakage, filling losses and heat transfer effects in the accurate prediction of efficiency and mass flow rate [1, 34, 36]. For a well designed machine, however, the influence of these factors on the rotor forces is expected to be relatively small, and in order to perform a general investigation of the effect of machine geometry on key operating parameters a simple 0D chamber model has been applied with the following assumptions:

- The working fluid is an ideal gas with $\gamma = 1.4$,
- The compression is an adiabatic process,
- There is no leakage into or out of working chambers,
- There are no filling or discharge pressure losses,
- Matched compression occurs (i.e. there is no difference between the pressure of the downstream gas, p_{dis}, and working chamber at the end of the compression process).

Using these assumptions, the variation in working chamber pressure, p_{wc}, can be calculated as a function of volume for a specified rotor geometry and value of built-in volume ratio (the ratio of maximum to minimum working chamber volume during compression), ε_v, as illustrated in Figure 10. Details of the port geometry do not need to be considered in this study as the porting losses are neglected. The rotor forces and torques due to a single working chamber can then be found using Eqns. 9-15 for straight or helical rotors. The results obtained are discussed in more detail in the following section.

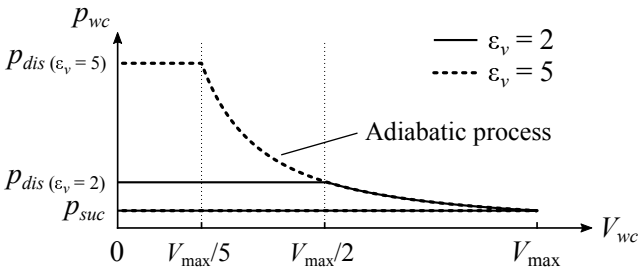

Fig. 10: Illustration of p-V diagram showing constant pressure filling and discharge with adiabatic compression process (subscripts *suc* and *dis* refer to the suction and discharge conditions of the working fluid)

4.4 Net rotor forces and torques

Once the forces and torques exerted on the rotor by a single working chamber have been found, the cumulative effect of all existing working chambers can be considered. The resulting net torques and forces vary periodically, with angular frequency $N_1\omega_1$. For the period $\phi_{1,i} \leq \phi_1 \leq (\phi_{1,i} + 2\pi/N_1)$, the net torques and forces due to all working chambers present in the machine can be found as shown for general cases in Eqn. 16. For values of $j > n$ or $j < 0$ the corresponding working chamber does not exist within the stated range of ϕ_1 values, and so does not influence the net forces or torques. Examples of the torque produced on the inner and outer rotors by a single working chamber, and the net torque due to all existing working chambers are shown in Fig. 11.

$$(T)_{net} = \sum_{j=0}^{n} T(\phi_1 + 2\pi j/N_1) \quad \text{and}$$

$$(F)_{net} = \sum_{j=0}^{n} F(\phi_1 + 2\pi j/N_1) \quad \text{where}$$

$$n = \lfloor (\phi_{1,f} - \phi_{1,i})\, N_1/2\pi \rfloor \qquad (16)$$

As a numerical approach has been used to generate the rotor profiles and find the resulting working chamber geometry and

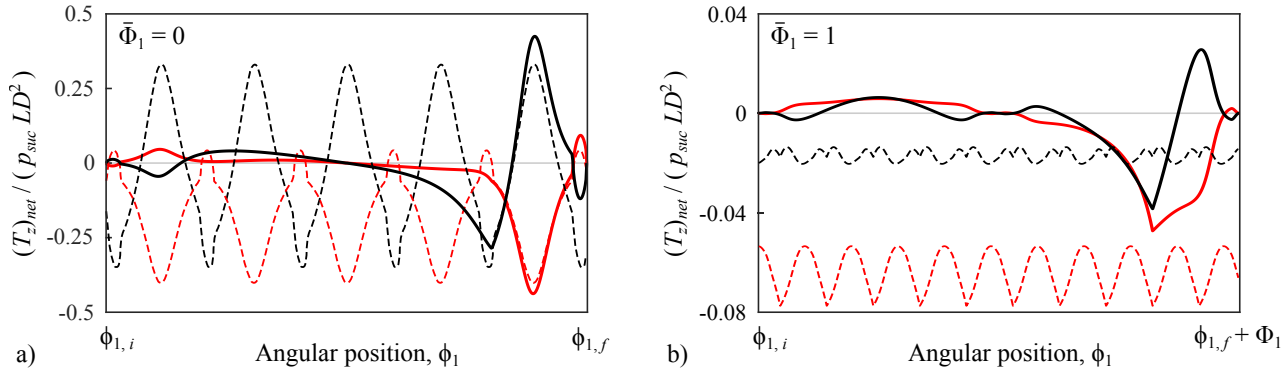

Fig. 11: Illustration of torque due to single working chamber (solid) and the net torque (dashed) on both inner (red) and outer (black) rotors for a) $\bar{\Phi}_1 = 0$ and b) $\bar{\Phi}_1 = 1$, when $N_1 = 5$, $\varepsilon_v = 5$, $\bar{\sigma} = 1$, $\lambda = 1.32$

rotor forces, it is possible to check the accuracy of this method using calculated torques such as those shown in Fig. 11. The assumptions used to calculate the working chamber pressure lead to the simple analytical expression for work done per cycle shown in Eqn. 17. The time-averaged power input, $\bar{P}_{in}$, should then be equal to the total power transferred from both rotors to the fluid, as shown in Eqn. 18, where $\bar{T}$ is the time-averaged value of the net rotor torque assuming constant speed. While greater numerical accuracy can be achieved by increased the number of coordinates per lobe, in all cases presented here the derived power values were found to agree with the analytical solution to within 0.1%.

$$W_{cyc} = \left(\frac{\gamma}{\gamma - 1}\right)\left(p_{dis}\frac{V_{max}}{\varepsilon_v} - p_{suc}V_{max}\right) \tag{17}$$

$$\bar{P}_{in} = W_{cyc}\left(\frac{N_1\omega_1}{2\pi}\right) = \omega_1(\bar{T}_1 + m_{21}\bar{T}_2) \tag{18}$$

There are two things to consider when comparing the results shown in Fig. 11 for different values of $\bar{\Phi}_1$. Firstly, it is the average torque that will determine average power, so although the maximum absolute values are different by an order of magnitude, the average values are considerably closer. Secondly, as the results are normalised by a factor of LD^2, if the same rotor length and maximum profile diameter are used, Fig. 9a shows that the straight rotors ($\bar{\Phi}_1 = 0$) will have more than twice the swept volume of the helical case ($\bar{\Phi}_1 = 1$). The end result is that the specific power is identical in the two cases, as would be expected when assuming adiabatic compression with no losses.

The results in Fig. 11 also illustrate that with straight rotors it is possible for the torque on each rotor to oscillate between positive and negative values, meaning that whichever rotor is connected to the motor, there are periods when the power transferred between the rotors is greater than the input power. Applying twist to the rotors is seen to reduce the relative fluctuations in torque, allowing at least one rotor to have torque acting in a single direction. The influence of rotor profile and wrap angle on the power transfer is discussed in the following section.

4.5 Power transfer between rotors

The instantaneous power transferred between a rotor and the working fluid is defined as $P_r = \omega_r T_r$ (where $r = 1$ or 2 depending on rotor). When losses are neglected, the total instantaneous power input to the compressor is equal to the sum of the power transferred from the two rotors to the fluid, $P_{in} = P_1 + P_2$. The proportion of this input power that is transferred to the fluid via each rotor is then related to the gear ratio, m_{21}, and the ratio of the net rotor torques, as defined in Eqn. 19. It is preferable to minimise the power transfer between the rotors, as this is a key factor in reducing stress in the contact regions, thereby limiting surface wear and frictional losses. In a compressors, one of the two rotors must be connected to a motor or other power supply. As P_r and P_{in} are functions of the rotor torques, and hence vary with time, this driven rotor should be the one with the largest instantaneous magnitude of this power ratio occurring during operation, as described in Eqn. 20. This ensures that the highest proportion of input power is transferred directly from the driven rotor to the fluid, rather than via the idle rotor.

The use of fixed-speed asynchronous motors is common in compressor applications. If the driven rotor is assumed to have a fixed rotational speed, then it is useful to consider any comparison of machine geometries on the basis of the induced volume per revolution of the driven rotor, $\bar{V}_{dr}$, as shown in Eqn. 21, rather than the standard swept volume per revolution of the outer rotor, $\bar{V}_{sw}$, defined in Section 3.1.1. The ideal volumetric flow rate of a machine can easily be found by multiplying $\bar{V}_{dr}$ by a chosen driven rotor speed, ω_{dr}; it is therefore possible to compare different configurations with different values of ω_{dr} if required.

$$\frac{P_2}{P_{in}} = 1 - \frac{P_1}{P_{in}} = \left(1 + \frac{P_1}{P_2}\right)^{-1} = \left(1 + \frac{(T_1)_{net}}{m_{21}(T_2)_{net}}\right)^{-1} \tag{19}$$

$$\text{Driven rotor} = \begin{cases} 1 \text{ (outer)}, & \text{if } \max(P_1/P_{in}) > \max(P_2/P_{in}) \\ 2 \text{ (inner)}, & \text{otherwise} \end{cases} \tag{20}$$

$$\bar{V}_{dr} = \bar{V}_{sw}\frac{N_{dr}}{N_1} \tag{21}$$

The sign of the instantaneous power transfer between the working fluid and rotors determines the nature of the power flow in the machine, with different modes of operation as defined in Fig. 12. Due to the fluctuations in the net rotor torques, operation of the compressor may be either entirely in the power-split or power-recirculation modes, or may alternate between them. This is illustrated by considering the examples in Fig. 11; for the case with straight rotors ($\bar{\Phi}_1 = 0$), whichever rotor is chosen

to drive the compressor, there are periods when the torques are both negative (corresponding to power-split), $T_{dr} < 0$ while $T_{id} > 0$ (corresponding to positive recirculation), and $T_{dr} > 0$ while $T_{id} < 0$ (corresponding to negative recirculation). The helical case with $\bar{\Phi}_1 = 1$ is seen to always operate in power-split mode, and in this particular case, the inner rotor should be used to drive the machine in order to minimise power transfer between the rotors. In general, negative recirculation should be

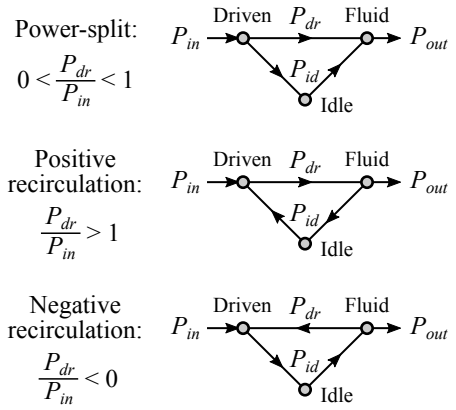

Fig. 12: Schematic illustration of power-split and power-recirculation operating modes for the transfer of power from the input shaft to the discharged fluid via the driven and idle rotors

avoided as this will always result in more power being transferred between rotors than is supplied to the machine. This can also occur with positive recirculation if $|P_{id}| > |P_{dr}/2|$. Minimising the power transfer between rotors requires the machine to operate in power-split and/or positive recirculation modes with $|P_{id}/P_{in}| \ll 1$. Identifying rotor geometries required to achieve this is discussed in the next section.

5 Geometrical optimisation for swept volume and power transfer objectives

During compressor operation, the maximum magnitude of the proportion of input power transferred to the idle rotor, $\Pi_{|\max|}$ (Eqn. 22), is a function of N_1, λ, $\bar{\sigma}$, $\bar{\Phi}_1$ (all of which also influence the swept volume of the machine) and ε_v. This is illustrated in Fig. 13, where the results for inner and outer driven rotors are only shown in the regions where they achieve the lower value of $\Pi_{|\max|}$.

$$\Pi_{|\max|} = \max \left| \frac{P_{id}}{P_{in}} \right| \tag{22}$$

The compromise between maximising the swept volume and minimising power transfer between rotors is illustrated in Fig. 14. This shows the results of a multi-variable optimisation using input parameters N_1, λ and $\bar{\Phi}_1$, and with objectives to maximise $\bar{V}_{dr}$ while minimising $\Pi_{|\max|}$. The Pareto frontiers showing the relationship between these two objectives have been obtained for machines with N_1 values between 3 and 6, and with either inner or outer rotors driven, and are shown in Fig. 15. The influence of $\bar{\sigma}$ has also been considered, and the Pareto optimal conditions were found to correspond to the maximum possible pin size (i.e. $\bar{\sigma} = 1$) in all cases. The results in Figs. 14 and 15 show that the compression ratio required in the application has a strong influence on the minimised power transfer between the rotors and the optimal rotor geometry. In all cases it can be seen that the maximum achievable $\bar{V}_{dr}$ values are lower when the inner rotor is driven. This difference is largely due to the assumption of constant driven rotor speed, which reduces the speed of the outer rotor due to the gearing ratio, m_{21}. For both values of ε_v considered, the minimum power transfer between rotors is achieved when the inner rotor is driven. For a particular value of N_1, and with either the inner or outer rotor driven, Fig. 15 indicates a general trend of increasing power transfer ratio with increasing $\bar{V}_{dr}$. It can however be seen that in many cases these curves do not increase continuously. The range of optimal solutions allows the rotor geometry to be specified in order to achieve the maximum possible value of $\bar{V}_{dr}$ for a given value of $\Pi_{|\max|}$.

5.1 Examples of optimised rotors

The results presented in Fig. 15 allow optimal geometries to be identified for the two values of ε_v considered. This requires a decision to be made on the relative importance of maximizing $\bar{V}_{dr}$ and minimising $\Pi_{|\max|}$. Examples are shown

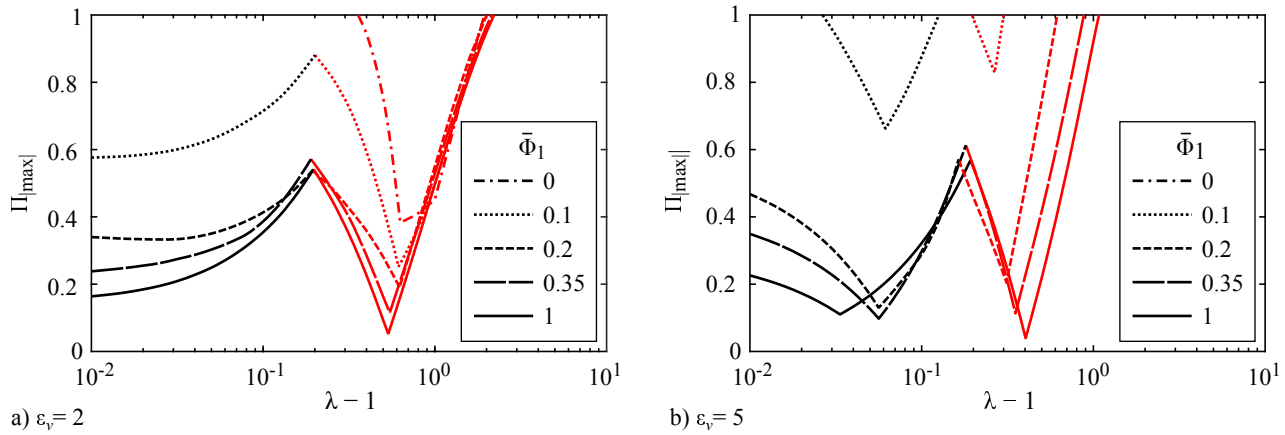

Fig. 13: Maximum proportion of input power transferred to idle rotor, $\Pi_{|\max|}$, as a function of λ and $\bar{\Phi}_1$, when the driven rotor is the inner (red) or outer (black); results are shown for the case when a) $\varepsilon_v = 2$ and b) $\varepsilon_v = 5$, with $N_1 = 5$, $\bar{\sigma} = 1$

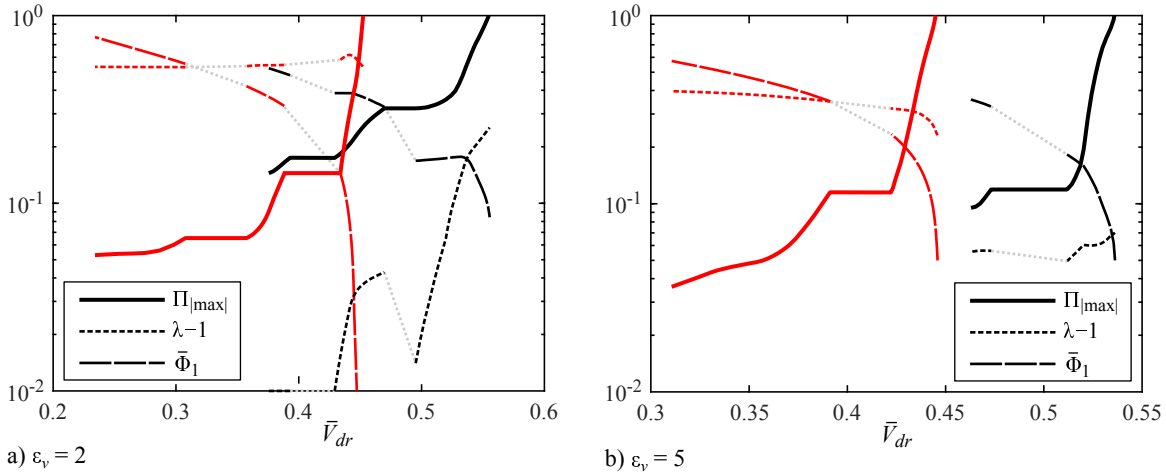

Fig. 14: Pareto frontiers showing the optimal solutions for minimising $\Pi_{|\max|}$ while maximising $\bar{V}_{dr}$, with inner driven (red) or outer driven (black) rotor when $N_1 = 5$ and $\varepsilon_v = 2$ & 5; the corresponding optimal values of λ (limited to a minimum value of 1.01) and $\bar{\Phi}_1$ are also shown, while $\bar{\sigma} = 1$ is optimal for all cases

in Tab. 1 and Fig. 16 for cases when the minimum possible values of $\Pi_{|\max|}$ are achieved with either inner or outer rotor driven. When considering the design of a machine for a particular application, this data allows the required swept volume to be achieved by selecting appropriate values of L and D. The required generating pin diameter and radius can then be found, and the geometry of both rotors is completely defined. For a particular case, the pitch length, L_p, of the inner and outer rotors is the same and can be found as shown in Eqn. 23.

$$L_p = \frac{2\pi L}{N_1 \Phi_1} \tag{23}$$

The results indicate that the optimised machines with outer driven rotors can achieve both higher normalised swept volume and have lower pitch point pressure angles compared to the cases with inner driven rotors, although these advantages are only achieved at the cost of significantly higher power transfer between the rotors. The outer driven machines have optimum values of λ which are significantly lower than for the inner driven cases, corresponding to smaller σ values (see Fig. 7), and resulting in a smaller radial offset and radius for the generating pin (see Tab. 1). There is also a large variation in the optimum values of the wrap angle. These results confirm that careful consideration of the proposed application and optimisation of the rotor geometry is necessary for any practical internally-geared screw machine.

An important point to note is that the optimisation objectives in this study, $\bar{V}_{dr}$ and $\Pi_{|max|}$, are independent of the actual values of rotor length and diameter. These values of L and D will, however, influence leakage and port flow areas, meaning that performance metrics such as volumetric and isentropic efficiency should also be considered. Future work is planned

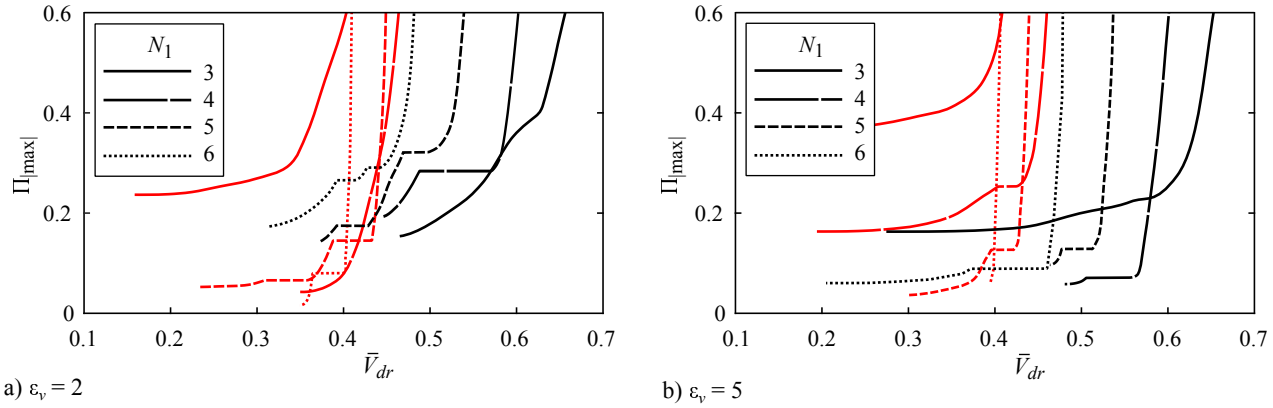

Fig. 15: Pareto frontiers for inner driven (red) or outer driven (black) rotor when $\varepsilon_v = 2$ & 5 , with $N_1 = 3-6$ and considering profiles with $\lambda \geq 1.01$ and wrap angles in the range $0 \leq \bar{\Phi}_1 \leq 1$

Table 1: Characteristics of internal screw geometry for cases with minimum possible $\Pi_{|\max|}$ when either inner or outer rotor is driven.

Case:	N_1	a/D	ρ/D	E/D	Φ_1 (deg)	L_p/L	α_p (deg)	$\bar{V}_{dr}$	$\Pi_{\|\max\|}$
Inner driven, $\varepsilon_v = 2$	6	0.625	0.274	0.074	136	0.441	28.2	0.35	0.018
Outer driven, $\varepsilon_v = 2$	3	0.327	0.042	0.108	233	0.515	0.7	0.46	0.154
Inner driven, $\varepsilon_v = 5$	5	0.629	0.309	0.090	209	0.344	20.2	0.30	0.037
Outer driven, $\varepsilon_v = 5$	4	0.413	0.108	0.098	183	0.492	4.3	0.48	0.056

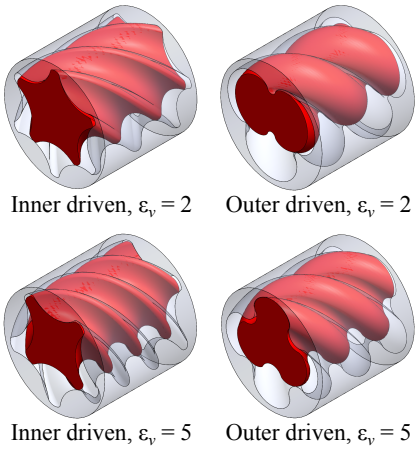

Fig. 16: Illustration of rotor geometries optimised for minimum power transfer, as described in Tab. 1 (note all cases are shown with $L/D = 1$)

to assess the relative importance of these factors. A key challenge will be the manufacture of rotors to the tight tolerances required to limit leakage flows for gas compression applications. The inner rotor is similar to conventional twin-screw rotors and is expected to be relatively easy to manufacture with high accuracy. The outer rotor is however more challenging, and a thorough investigated of possible rotor materials and manufacturing methods is planned. Detailed design work is also necessary to assess the practicality of the required bearing and seal arrangements for inner or outer driven machine configurations.

6 Conclusions

This study has shown that internally-geared machines with fixed end face porting can be designed to achieve low transfer of power between the rotors while maintaining relatively high swept volume. The main conclusions can be summarised as follows:

- Applying twist to internally-geared rotors with constant pitch and profile enables a significant reduction in the power transferred between rotors during operation when compared to straight-cut rotors.
- With other parameters fixed, increasing either the wrap angle of rotors, or the number of lobes, reduces the normalised working chamber volume. This tends to reduce both the proportion of input power transferred between rotors and the volume created per revolution of the driven rotor, but the required pressure ratio is also an important factor in determining the minimum achievable power transfer ratio in each case.
- Rotor profiles generated using the maximum possible pin size that avoids undercutting, $\sigma = \sigma_{lim}(N_1, \lambda)$, are found to achieve Pareto optimal results for the swept volume and power transfer ratio objectives.
- For the compressor applications considered, inner driven rotors are predicted to be capable of achieving lower power transfer ratios, but the gearing ratio between rotors means that outer driven machines tend to have a higher swept volume per revolution of the driven rotor.
- When seeking to minimise the power transfer ratio, the required pressure ratio of the machine and the choice of driven rotor are shown to lead to significantly different optimum profiles and wrap angles.

Further work is needed to understand how the rotor geometry influences the port geometry and leakage areas. An improved model of the filling, compression and discharge processes will allow more accurate predictions of the working chamber pressure and hence the forces and torques exerted on the rotors. The prediction of mass flow rate and efficiency of the machine for particular applications will introduce additional optimisation objectives. For example, minimising the specific power for particular compressor applications is likely to lead to compromises in either swept volume or power transfer between rotors. Characterisation of these compromises is an important step in understanding the potential value of this novel machine configuration.

Nomenclature

a Radial distance to pin centre (m)
A Area (m^2)
D Maximum rotor profile diameter (m)
E Distance between rotor axes (m)
L Rotor length (m)
L_p Pitch length of the helical rotors (m)
m_{21} Gearing ratio of rotors, defined as ω_2/ω_1
N Number of lobes on rotor
p Pressure (bar)
P Instantaneous power transfer between rotor and fluid (W)
P_{in} Instantaneous machine input power via driven rotor (W)
r Centrode radius (m)
T Torque (Nm)
$\bar{T}$ Time-averaged net rotor torque (Nm)
V Volume (m^3)
V_{sw} Swept volume of machine per revolution of outer rotor (m^3)
$\bar{V}_{dr}$ Normalised swept volume for the driven rotor (-)
α_p Pressure angle for contact at pitch point (rad)
ρ Radius of pin (m)
ω Angular speed (rad/s)
ϕ Angular position of rotor (rad)
Φ Wrap angle of rotor (rad)
ε_v Built-in volume ratio, i.e. ratio of max to min volume for compression process (-)
ψ Rotor profile
λ Normalised radial distance to pin centre (-)
σ Normalised radius of pin (-)
σ_{lim} Maximum possible normalised radius of pin (-)
$\bar{\sigma}$ Pin radius relative to maximum possible value (-)
$\Pi_{|\max|}$ Maximum proportion of input power transferred between rotors (-)

Subscripts:

1, 2 Outer or inner rotor respectively

net Net result of all existing working chambers

p, q Pin or fillet sections of outer rotor respectively

dr, *id* Driven or idle rotor respectively

ℓ, t Leading or trailing contact point of working chamber

suc, *dis* Working fluid conditions in the suction or discharge port of the compressor

References

[1] Rundo, M., 2017. "Models for flow rate simulation in gear pumps: A review". *Energies,* **10**(9), p. 1261.

[2] Cholet, H., 1997. *Progressing Cavity Pumps*. Editions Technips.

[3] Moineau, R., 1934. "Gear mechanism". *U.S. Patent 1,892,217*.

[4] Adams, G., and Beard, J., 1997. "Comparison of helical and skewed axis gerotor pumps". *Mechanism and Machine Theory,* **32**(6), pp. 729–742.

[5] Dmitriev, O., and Arbon, I., 2017. "Comparison of energy-efficiency and size of portable oil-free screw and scroll compressors". In IOP Conference Series: Materials Science and Engineering, Vol. 232, IOP Publishing.

[6] Read, M., Smith, I., and Stosic, N., 2017. "Internally geared screw machines with ported end plates". In IOP Conference Series: Materials Science and Engineering, Vol. 232, IOP Publishing.

[7] Read, M., Stosic, N., and Smith, I., 2017. "Operational characteristics of internally geared positive displacement screw machines". In ASME International Mechanical Engineering Congress and Exposition, American Society of Mechanical Engineers, pp. V006T08A032–V006T08A032.

[8] Read, M., Stosic, N., and Smith, I., 2018. "Port flow losses in internally geared positive displacement machines". In 24th International Compressor Engineering Conference at Purdue.

[9] Colbourne, J., 1974. "The geometry of trochoid envelopes and their application in rotary pumps". *Mechanism and Machine Theory,* **9**(3).

[10] Beard, J., Hall, A., and Soedel, W., 1991. "Comparison of hypotrochoidal and epitrochoidal gerotors". *Journal of Mechanical Design,* **113**, pp. 133–141.

[11] Beard, J., Yannitell, D., and Pennock, G.", 1992.".

[12] Shung, J., and Pennock, G., 1994. "Geometry for trochoidal-type machines with conjugate envelopes". *Mechanism and Machine Theory*(1), pp. 25–42.

[13] Tong, S., Yan, J., and Yang, D., 2009. "Design of deviation-function based gerotors". *Mechanism and Machine Theory,* **44**(8), pp. 1595–1606.

[14] Yan, J., Yang, D., and Tong, S., 2009. "A new gerotor design method with switch angle assignability". *Journal of Mechanical Design,* **131**(1). 011006.

[15] Hsieh, C., and Hwang, Y., 2007. "Geometric design for a gerotor pump with high area efficiency". *Journal of Mechanical Design,* **129**(12), pp. 1269–1277.

[16] Hsieh, C., 2009. "Influence of gerotor performance in varied geometrical design parameters". p. 121008.

[17] Hsieh, C., 2012. "Fluid and dynamics analyses of a gerotor pump using various span angle designs". *Journal of Mechanical Design,* **134**(12), p. 121003.

[18] Bonandrini, G., Mimmi, G., and Rottenbacher, C., 2009. "Theoretical analysis of internal epitrochoidal and hypotrochoidal machines". *Proceedings of the Institution of Mechanical Engineers, Part C: Journal of Mechanical Engineering Science,* **223**(6), pp. 1469–1480.

[19] Mimmi, G., and Pennacchi, P., 1997. "Rotor design and optimization in internal lobe pumps". *Applied Mechanics Reviews,* **50**, pp. S133–S141.

[20] Bae, J., Kwak, H., San, S., and Kim, C., 2016. "Design and cfd analysis of gerotor with multiple profiles (ellipseinvoluteellipse type and 3-ellipses type) using rotation and translation algorithm". *Proceedings of the Institution of Mechanical Engineers, Part C: Journal of Mechanical Engineering Science,* **230**(5), pp. 804–823.

[21] Hao, C., Wenming, Y., and Guangming, L., 2016. "Design of gerotor oil pump with new rotor profile for improving performance". *Proceedings of the Institution of Mechanical Engineers, Part C: Journal of Mechanical Engineering Science*(4), pp. 592–601.

[22] Jacazio, G., and Martin, A. D., 2016. "Influence of rotor profile geometry on the performance of an original low-pressure gerotor pump". *Mechanism and Machine Theory,* **100**, pp. 296–312.

[23] Litvin, F., and Feng, P., 1996. "Computerized design and generation of cycloidal gearings". *Mechanism and Machine Theory,* **31**(7), pp. 891–911.

[24] Vecchiato, D., Demenego, A., Argyris, J., and Litvin, F., 2001. "Geometry of a cycloidal pump". *Computer methods in applied mechanics and engineering,* **190**(18), pp. 2309–2330.

[25] Mimmi, G., and Pennacchi, P., 2000. "Non-undercutting conditions in internal gears". *Mechanism and Machine Theory,* **35**(4), pp. 477–490.
[26] Mathias, J., Johnston, J., Cao, J., Priedeman, D., and Christensen, R.", 2009.". *Journal of Energy Resources Technology,* **131**(1), p. 012201.
[27] Gamez-Montero, P., Castilla, R., Mujal, R., Khamashta, M., and Codina, E., 2009. "Gerolab package system: Innovative tool to design a trochoidal-gear pump". *Journal of Mechanical Design,* **131**(7), p. 074502.
[28] Gamez-Montero, P., Garcia-Vilchez, M., Raush, G., Freire, J., and Codina, E., 2012. "Teeth clearance and relief grooves effects in a trochoidal-gear pump using new modules of gerolab". *Journal of Mechanical Design,* **134**(5), p. 054502.
[29] Demenego, A., Vecchiato, D., Litvin, F., Nervegna, N., and Manc, S., 2002. "Design and simulation of meshing of a cycloidal pump". *Mechanism and Machine Theory,* **37**(3), pp. 311–332.
[30] Ivanović, L., Devedžić, G., Ćuković, S., and Mirić, N., 2012. "Modeling of the meshing of trochoidal profiles with clearances". *Journal of Mechanical Design,* **134**(4), p. 041003.
[31] Robison, A., and Vacca, A., 2018. "Multi-objective optimization of circular-toothed gerotors for kinematics and wear by genetic algorithm". *Mechanism and Machine Theory,* **128**, pp. 150–168.
[32] Bonandrini, G., Mimmi, G., and Rottenbacher, C., 2012. "Design and simulation of meshing of a particular internal rotary pump". *Mechanism and Machine Theory,* **49**, pp. 104–116.
[33] Hsieh, C., 2015. "Flow characteristics of gerotor pumps with novel variable clearance designs". *ASME Journal of Fluids Engineering,* **137**(4), p. 041107.
[34] Stosic, N., Smith, I., and Kovacevic, A., 2005. *Screw compressors: mathematical modelling and performance calculation*. Springer Science & Business Media.
[35] Adams, G., and Soedel, W., 1995. "Computation of compression loads in twin screw compressors". *Journal of Mechanical Design,* **117**(4), pp. 512–519.
[36] Hanjalic, K., and Stosic, N., 1997. "Development and optimization of screw machines with a simulation model - part II: Thermodynamic performance simulation and design optimization". *Journal of Fluids Engineering,* **119**(3), pp. 664–670.